Journal of Zhejiang University SCIENCE A
ISSN 1673-565X (Print); ISSN 1862-1775 (Online)
www.zju.edu.cn/jzus; www.springerlink.com
E-mail: jzus@zju.edu.cn

# Impact of load impedance on the performance of a thermoacoustic system employing acoustic pressure amplifier*

Ke TANG†, Zhong-jie HUANG, Tao JIN†‡, Guo-bang CHEN

(*Institute of Refrigeration and Cryogenics, Zhejiang University, Hangzhou 310027, China*)

†E-mail: ktang@zju.edu.cn; jintao@zju.edu.cn

Received June 10, 2007; revision accepted Sept. 5, 2007; published online Dec. 14, 2007

**Abstract:** An acoustic pressure amplifier (APA) is capable of improving the match between a thermoacoustic engine and a load by elevating pressure ratio and acoustic power output. A standing-wave thermoacoustic engine driving a resistance-and-compliance (RC) load through an APA was simulated with linear thermoacoustics to study the impact of load impedance on the performance of the thermoacoustic system. Based on the simulation results, analysis focuses on the distribution of pressure amplitude and velocity amplitude in APA with an RC load of diverse acoustic resistances and compliance impedances. Variation of operating parameters, including pressure ratio, acoustic power, hot end temperature of stack, etc., versus impedance of the RC load is presented and analyzed according to the abovementioned distribution. A verifying experiment has been performed, which indicates that the simulation can roughly predict the system operation in the fundamental-frequency mode.

**Key words:** Thermoacoustic engine, Acoustic pressure amplifier (APA), Thermoacoustics
**doi:**10.1631/jzus.A071340 **Document code:** A **CLC number:** O424

## INTRODUCTION

In recent years, much effort has been made to enhance the performance of thermoacoustic refrigeration systems by ameliorating the match between a thermoacoustic engine and a load (say a pulse tube cooler) (Arman *et al*., 2003; Duthil *et al*., 2006; Matsubara *et al*., 2003; Nguyen *et al*., 2004; Tang *et al*., 2004; 2005; 2006; Yu *et al*., 2007). An acoustic pressure amplifier (APA), a long circular tube, was introduced to thermoacoustic systems in 2005 (Dai *et al*., 2005). Significantly elevated pressure ratio (maximum pressure divided by minimum pressure of a pressure oscillation) and acoustic power output, deriving from this novel configuration, led to a marked improvement of the system's performance, such as a lower no-load cooling temperature and an increased cooling capacity (Bao *et al*., 2006a; Dai *et al*., 2005; Hu *et al*., 2007; Tang *et al*., 2007).

This study focuses on the impact of load impedance on the performance of a thermoacoustic system to analyze the match between the engine and the load through an APA. A standing-wave thermoacoustic engine driving a resistance-and-compliance (RC) load through an APA was simulated with linear thermoacoustics. According to the simulation results, variation of operating parameters, including pressure ratio, acoustic power, hot end temperature of stack, etc., versus acoustic resistance and compliance impedance of the RC load is presented and analyzed. Different impedance characteristics of RC load for the maximum acoustic power output are discussed, compared with previous work on the thermoacoustic system without an APA (Bao *et al*., 2006b). Experiment has also been performed to verify the simulation results.

‡ Corresponding author

* Project supported by the National Natural Sciences Foundation of China (No. 50536040), the University Doctoral Subject Special Foundation of China (No. 20050335047), the Postdoctoral Science Foundation of Zhejiang Province (No. 2006-bsh-21), and the Natural Science Foundation of Zhejiang Province (No. Y107229), China

## SIMULATION

According to linear thermoacoustics (Swift, 2002), the momentum, continuity and energy equations for a short channel are as follows:

$$\frac{\mathrm{d}p_1}{\mathrm{d}x}=-(\mathrm{i}\omega l+r_v)U_1, \tag{1}$$

$$\frac{\mathrm{d}U_1}{\mathrm{d}x}=-(\mathrm{i}\omega c+1/r_\kappa)p_1+eU_1, \tag{2}$$

$$\frac{\mathrm{d}T_\mathrm{m}}{\mathrm{d}x}=\left\{\dot{H}_2-\frac{1}{2}\mathrm{Re}\left[p_1\tilde{U}_1\left(1-\frac{f_\kappa-\tilde{f}_v}{(1+\xi)(1+Pr)(1-\tilde{f}_v)}\right)\right]\right\}$$
$$\cdot\left\{\frac{\rho_\mathrm{m}c_\mathrm{p}|U_1|^2}{2A\omega(1-Pr)|1-f_v|^2}\mathrm{Im}\left(\tilde{f}_v+\frac{(f_\kappa-\tilde{f}_v)(1+\xi f_v/f_\kappa)}{(1+\xi)(1+Pr)}\right)\right.$$
$$\left.-(AK+A_\mathrm{s}K_\mathrm{s})\right\}^{-1}, \tag{3}$$

$$l=\frac{\rho_\mathrm{m}}{A}\frac{1-\mathrm{Re}(f_v)}{|1-f_v|^2}, \tag{4}$$

$$c=\frac{A}{\gamma p_\mathrm{m}}\left[1+(\gamma-1)\mathrm{Re}\left(\frac{f_\kappa}{1+\xi}\right)\right], \tag{5}$$

$$r_v=\frac{\omega\rho_\mathrm{m}}{A}\frac{\mathrm{Im}[-f_v]}{|1-f_v|^2}, \tag{6}$$

$$r_\kappa=\frac{\gamma}{\gamma-1}\frac{p_\mathrm{m}}{\omega A\,\mathrm{Im}\left(-f_\kappa/(1+\xi)\right)}, \tag{7}$$

$$e=\frac{f_\kappa-f_v}{(1-f_v)(1-Pr)(1+\xi)}\frac{1}{T_\mathrm{m}}\frac{\mathrm{d}T_\mathrm{m}}{\mathrm{d}x}, \tag{8}$$

where $p_1$ and $U_1$ are pressure amplitude and volume velocity amplitude, $\omega$ is angular frequency, $\rho_\mathrm{m}$, $T_\mathrm{m}$, $c_\mathrm{p}$, $\gamma$, $K$ and $Pr$ are mean density, temperature, isobaric specific heat, specific heat ratio, thermal conductivity and Prandtl number of working fluid, respectively, $f_v$ and $f_\kappa$ are viscous function and thermal function (Swift, 2002), $A$ is flow area of channel, $A_\mathrm{s}$ and $K_\mathrm{s}$ are cross section area and thermal conductivity of the solid forming the channel, $\dot{H}_2$ is total power, $\xi$ is a quantity presenting the effect of specific heat and thermal conductivity of the channel solid on the heat transfer between the working fluid and the channel ($\xi$ equals zero for the ideal solid with infinite specific heat and thermal conductivity), i is imaginary unit, Re, Im and superscript '~' mean the real part, the imaginary part and the conjugation of a complex quantity. $l$, $c$, $r_v$, $r_\kappa$ and $e$ are inertance, compliance, viscous resistance, thermal-relaxation resistance and proportionality coefficient of a controlled source, which can be calculated with Eqs.(4)~(8).

The standing-wave thermoacoustic engine driving an RC load through an APA is schematically shown in Fig.1. The engine employs a symmetrical configuration. Main dimensions are listed in Table 1. The thermoacoustic system has been simulated with abovementioned linear thermoacoustics.

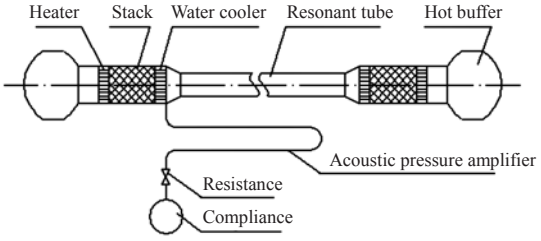


**Fig.1 Schematic of a standing-wave thermoacoustic engine driving an RC load through an APA**

**Table 1 Dimensions of standing-wave thermoacoustic engine**

| | Diameter (mm) | Length (mm) |
|---|---|---|
| Heater | 56 | 64 |
| Stack | 56 | 285 |
| Water cooler | 56 | 34 |
| Resonant tube | 36 | 8000 |
| Hot buffer | | (1.35 L) |

The APA is a long circular tube, and the viscous resistance in APA is corrected according to (Swift, 2002), since the oscillating flow is within the range of turbulence flow in the computed case. The dimensions of APA are fixed, i.e. 3.5 m in length and 8 mm in diameter, to concentrate emphasis on the influence of load impedance. The acoustic resistance and compliance impedance of the RC load, which derive from the viscosity of fluid in needle valve and the condensability of fluid in reservoir, respectively, are given as independent variables. Helium is adopted as working gas, heating power is 1.4 kW and working pressure is 2.6 MPa. A program was written to deal with the numerical computation. The velocity mentioned below is volumetric velocity.

## SIMULATION RESULT AND ANALYSIS

Distributions of pressure amplitude and velocity amplitude in APA, with different impedances of RC load, are computed and shown in Fig.2 and Fig.3, respectively. The normalized location of "0" stands for APA's inlet, i.e. the end connecting to the engine, and "1" for APA's outlet, i.e. the end to the RC load. In the case of an acoustic resistance of $1\times10^6$ Pa·s/m$^3$, the distributions are obviously influenced by compliance impedance of RC load. For relatively small compliance impedance, such as $-5\times10^7$i Pa·s/m$^3$ and $-1\times10^8$i Pa·s/m$^3$ (i is imaginary unit, and the so-called "small" or "large" is a description for the absolute value of compliance impedance), a minimum of pressure amplitude and a maximum of velocity amplitude exist in APA, almost at the same location. However, for relatively large compliance impedance, such as $-3\times10^8$i Pa·s/m$^3$ and $-5\times10^8$i Pa·s/m$^3$, pressure amplitude increases monotonously from the inlet to the outlet of APA, while velocity amplitude decreases. It is found that there is a critical compliance impedance of RC load between $-1\times10^8$i Pa·s/m$^3$ and $-3\times10^8$i Pa·s/m$^3$, for the occurrence of the minimum pressure amplitude and the maximum velocity amplitude. The situation for an acoustic resistance of $1\times10^9$ Pa·s/m$^3$ seems much simpler. Compliance impedance has little impact on the distributions, indicated by coincidence of the curves for different compliance impedances. A monotonous rise of pressure amplitude is also accompanied by a monotonous drop of velocity amplitude.

It is seen that the distribution characteristics are similar to that of a standing-wave acoustic field, and the minimum pressure amplitude means pressure node, while the maximum velocity amplitude is velocity antinode. The amplification effect of pressure ratio by APA originates from the distribution characteristics, which also significantly affect the variation of operating parameters versus impedance of RC load.

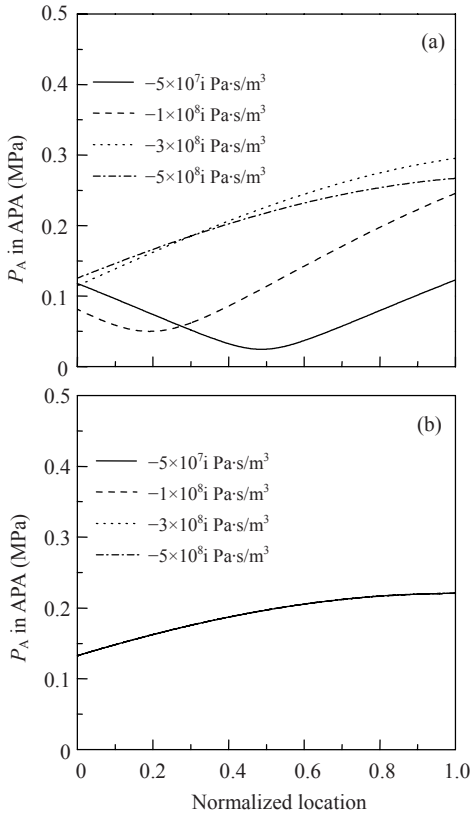


**Fig.2 Distribution of pressure amplitude in APA with different impedances of RC load**
(a) Acoustic resistance: $1\times10^6$ Pa·s/m$^3$; (b) Acoustic resistance: $1\times10^9$ Pa·s/m$^3$

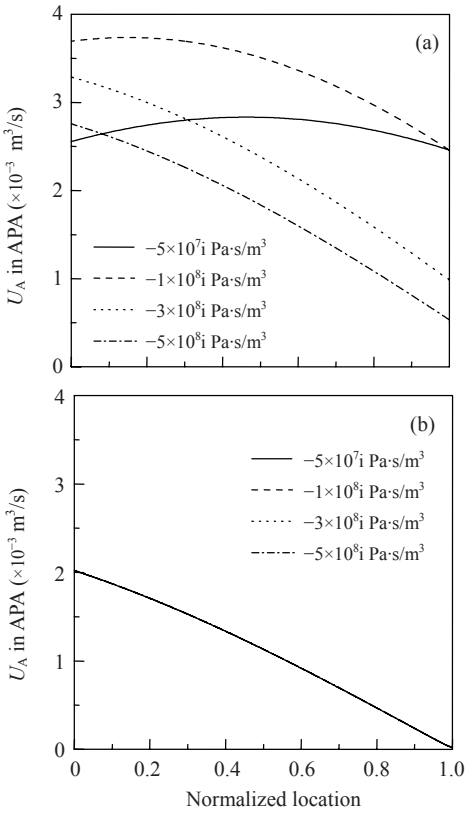


**Fig.3 Distribution of velocity amplitude in APA with different impedances of RC load**
(a) Acoustic resistance: $1\times10^6$ Pa·s/m$^3$; (b) Acoustic resistance: $1\times10^9$ Pa·s/m$^3$

Fig.4 shows the functions of pressure ratio at APA's outlet versus acoustic resistance of RC load with different compliance impedances. In the case of acoustic resistance below $1\times10^6$ Pa·s/m$^3$, compared with little influence of acoustic resistance, the change of compliance impedance leads to apparent variation of pressure ratio. In the range of compliance impedance below the abovementioned critical value, i.e. with a pressure node and a velocity antinode in APA, the pressure ratio at APA's outlet increases with a rise of compliance impedance, as shown in Fig.4a, which may be attributed to two aspects. One is that the rise of compliance impedance makes the pressure node approach to APA's inlet (Fig.2a), so there is a relatively long distance for the increasing procedure of pressure amplitude in APA. Moreover, the pressure ratio at APA's inlet is sustained by the engine, and the rise of compliance impedance leads to a little smaller pressure amplitude at APA's inlet but a larger pressure amplitude of pressure node. The other reason is that the approaching of pressure node and velocity antinode to APA's inlet reduces the impedance at the inlet, leading to larger velocity amplitude in APA (Fig.3a). Consequently, a higher increasing rate of pressure amplitude is achieved, indicated by the slopes of curves in Fig.2a. On the contrary, when compliance impedance is larger than the abovementioned critical value, leading to monotonous distributions of pressure and velocity amplitude in APA, the pressure node and velocity antinode deviate from APA's inlet with the rise of compliance impedance. Accordingly, the increased impedance at APA's inlet, derived from the deviation, results in smaller velocity amplitude and then also lower increasing rate of pressure amplitude in APA. Thus, in this case, pressure ratio at APA's outlet decreases with the rise of compliance impedance, as shown in Fig.4b. In short, a higher pressure ratio at APA's outlet is achieved near the abovementioned critical compliance impedance of RC load.

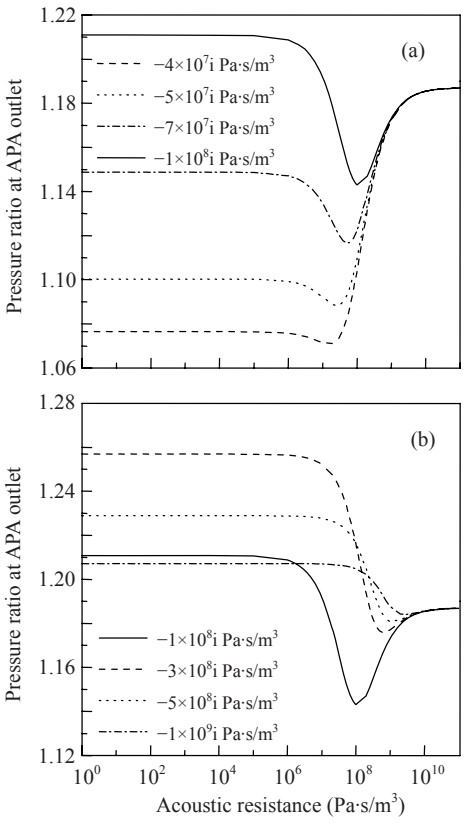


**Fig.4 Pressure ratio at APA's outlet versus impedance of RC load**

(a) Relatively small compliance impedance; (b) Relatively large compliance impedance

For acoustic resistances above $1\times10^9$ Pa·s/m$^3$, little difference is found between the curves for various compliance impedances. Such a large acoustic resistance restrains the influence of compliance impedance, and dominates the system operation. The increase of acoustic resistance leads to a slight rise of the pressure ratio at APA's outlet.

The acoustic resistance, between $1\times10^6$ Pa·s/m$^3$ and $1\times10^9$ Pa·s/m$^3$, is comparable to the compliance impedance of RC load, and both of them affect the pressure ratio at APA's outlet apparently. There exists a minimum pressure ratio with the rise of acoustic resistance, and the rise of compliance impedance leads to an increase of the minimum pressure ratio.

The variation of pressure ratio at APA's inlet, presented in Fig.5, is similar to that at APA's outlet. The difference is that for acoustic resistance of RC load below $1\times10^9$ Pa·s/m$^3$, the compliance impedance close to the forementioned critical value results in smaller pressure ratio at APA's inlet.

Fig.6 shows amplification ratio of APA, pressure amplitude at APA's outlet divided by pressure amplitude at APA's inlet. The amplification effect, indicated by amplification ratio above 1, can be achieved for most RC load impedances. However, an RC load of small acoustic resistance and compliance impedance may make pressure amplitude at APA's outlet smaller than that at APA's inlet (Fig.6a), and no amplification effect happens.

Acoustic power generation in stacks and losses

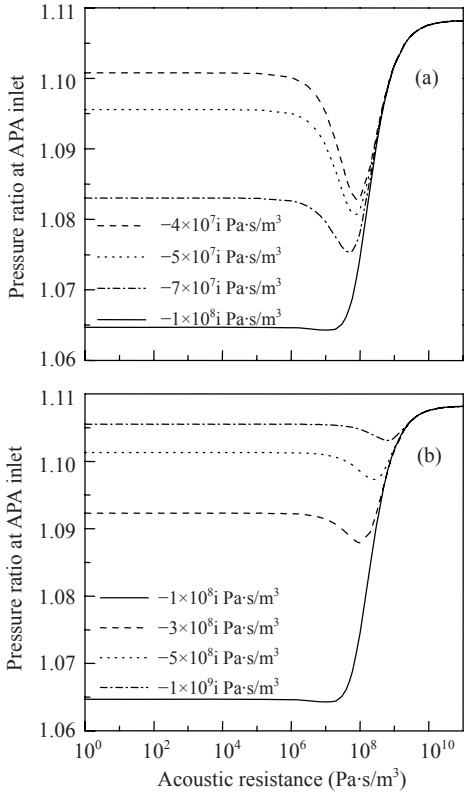


**Fig.5 Pressure ratio at APA's inlet versus impedance of RC load. (a) Relatively small compliance impedance; (b) Relatively large compliance impedance**

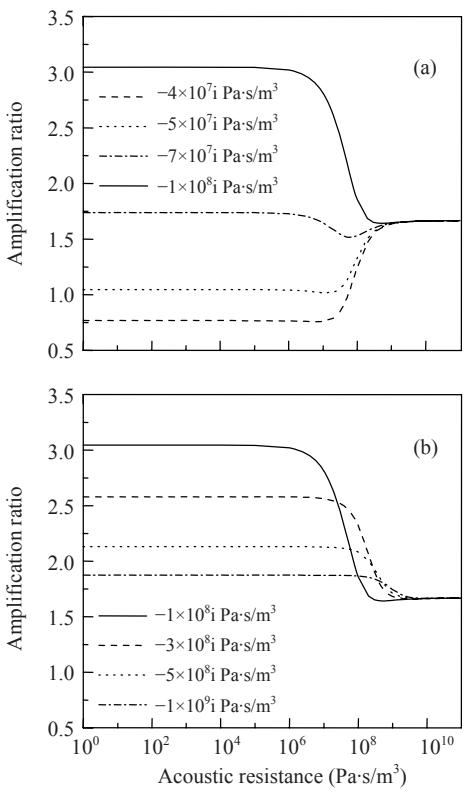


**Fig.6 Amplification ratio versus impedance of RC load. (a) Relatively small compliance impedance; (b) Relatively large compliance impedance**

in engine, APA and RC load have also been computed, which are presented in Figs.7~10, respectively, in order to get more information from the viewpoint of energy. The variations of acoustic power generation and losses in engine versus impedance of RC load are similar to those of pressure ratio at APA's inlet. Considerable acoustic power is consumed by APA in the case of acoustic resistance below $1\times10^6$ Pa·s/m$^3$, and a compliance impedance close to the critical value leads to more acoustic power consumption in APA. However, when the acoustic resistance is larger than $1\times10^9$ Pa·s/m$^3$, the acoustic power consumption in APA drops to below 20 W. There is an obvious "peak" of acoustic power delivered to RC load with the acoustic resistance between $1\times10^6$ Pa·s/m$^3$ and $1\times10^9$ Pa·s/m$^3$, and a relatively high "peak" is achieved with a compliance impedance below the critical value. Comparison of curves in the above figures indicates that considerable acoustic power delivered to the load and consumed in the APA causes a weakened oscillation in the engine, which leads to less acoustic power generation and losses in the engine, because the acoustic power generation derives from the amplification of volumetric velocity, and viscous loss and thermal-relaxation loss are proportional to squared velocity amplitude and squared pressure amplitude, respectively. Additionally, the weakened oscillation in the engine, especially the reduced velocity amplitude, deteriorates the heat transfer at the stack's hot end and causes considerably higher hot end temperature of stack, as shown in Fig.11. Such a high hot end temperature may limit the practical operation.

The impedance characteristics of RC load for maximum acoustic power output attracts our interest. Fig.10 indicates that for the compliance impedances below $-1\times10^8$i Pa·s/m$^3$, a maximum acoustic power output occurs at an acoustic resistance slightly larger than the compliance impedance, however, in the case of a compliance impedance above $-1\times10^8$i Pa·s/m$^3$, an acoustic resistance slightly smaller than the compliance impedance leads to a maximum acoustic power output. This is different from our previous

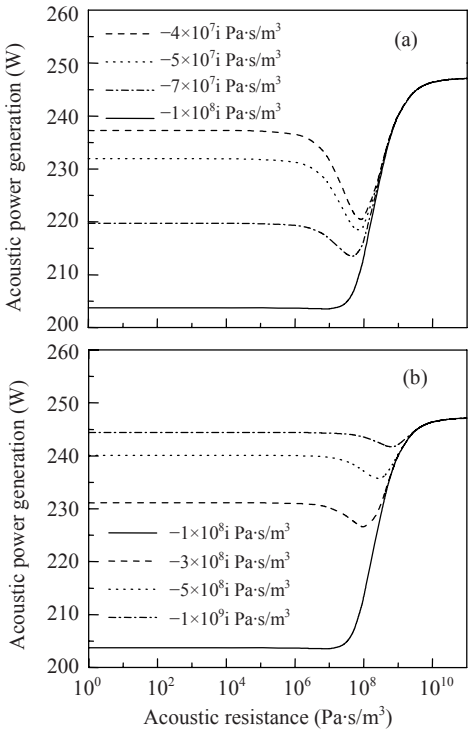


**Fig.7 Acoustic power generation versus impedance of RC load. (a) Relatively small compliance impedance; (b) Relatively large compliance impedance**

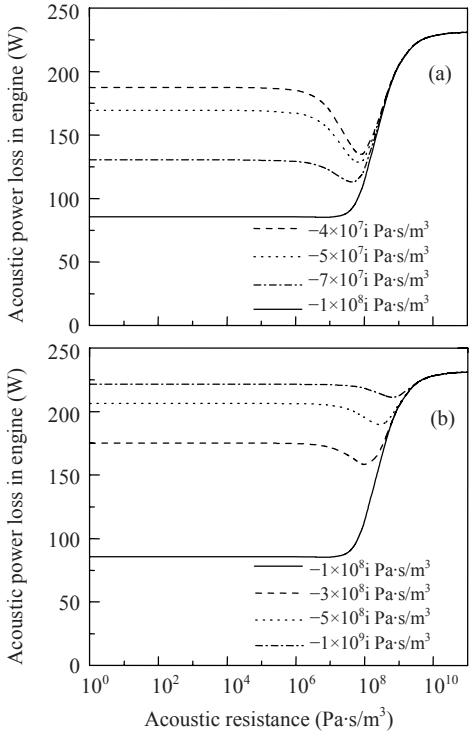


**Fig.8 Acoustic power loss in engine versus impedance of RC load. (a) Relatively small compliance impedance; (b) Relatively large compliance impedance**

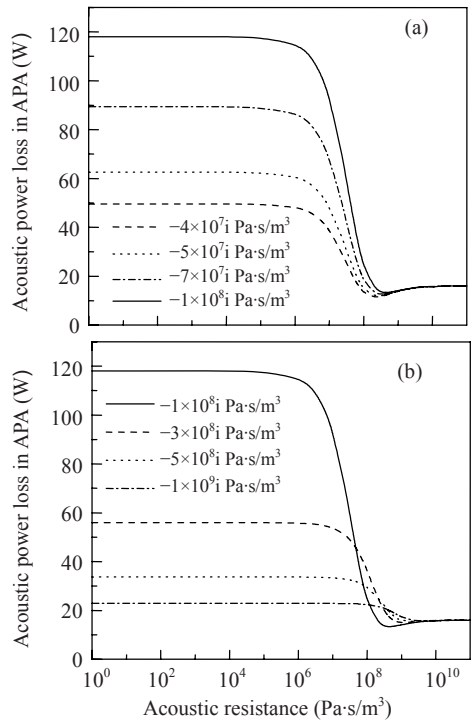


**Fig.9 Acoustic power loss in APA versus impedance of RC load. (a) Relatively small compliance impedance; (b) Relatively large compliance impedance**

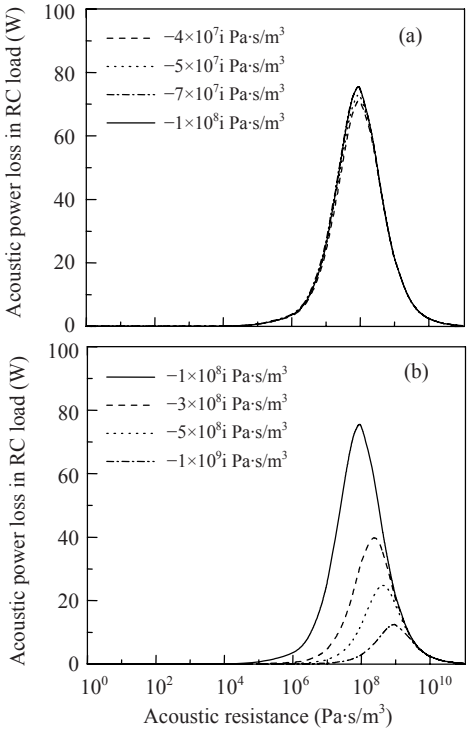


**Fig.10 Acoustic power loss in RC load versus impedance of RC load. (a) Relatively small compliance impedance; (b) Relatively large compliance impedance**

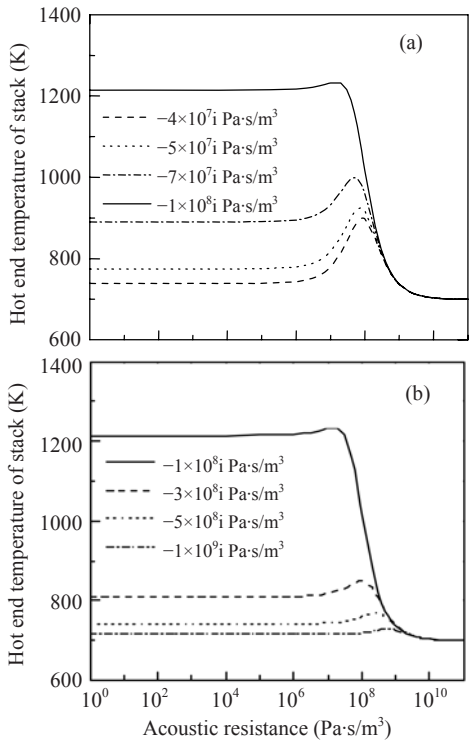


**Fig.11 Hot end temperature of stack versus impedance of RC load. (a) Relatively small compliance impedance; (b) Relatively large compliance impedance**

work on thermoacoustically driven RC load without APA (Bao *et al*., 2006b), in which maximum acoustic power output is achieved with an equivalent acoustic resistance and compliance impedance. The difference can be attributed to the marked variation of pressure ratio entering RC load with the load's impedance, due to the introduction of APA.

## EXPERIMENT AND VERIFICATION

In order to verify the simulation results, experiment on the standing-wave thermoacoustic engine driving an RC load through an APA has been performed. The APA is a long circular tube of 3.5 m in length and 8 mm in diameter. The RC load is composed of a needle valve and a reservoir. Two reservoirs of 260 $cm^3$ and 40 $cm^3$, whose compliance impedances are roughly $-6.0\times10^7$i Pa·s/$m^3$ and $-3.9\times10^8$i Pa·s/$m^3$, respectively, were tested in the experiment. Helium is adopted as working gas, heating power is 1.4 kW and working pressure is 2.6 MPa. Three pressure sensors are located at the joint of the engine and the APA, the outlet of APA to the needle valve, and the reservoir, respectively, and the acoustic power into the RC load can be estimated (Bao *et al*., 2006b).

Experimental data, together with corresponding computed results, including pressure ratio and phase difference of pressure waves at APA's outlet and inlet, acoustic power loss in the RC load, hot end temperature of left stack and operating frequency of the system, are presented in Figs.12~17, respectively. Comparison of the computed results and experimental data indicates that the simulation can roughly predict the variation of the system's operating parameters.

The data of phase difference of pressure waves at APA's outlet and inlet, as shown in Fig.14, may reflect some useful information of pressure amplitude distribution from the viewpoint of phase. The phase difference in the range of 0° to 90° indicates that the pressure wave at APA's outlet is approximately in phase with that at APA's inlet, so there is no pressure node in the APA according to the distribution characteristics of a standing wave. On the contrary, the phase difference in the range of 90° to 180° is relatively close to 180°, and there should be a pressure node in the APA. Thus, the data in Fig.14 indicates that for relatively large compliance impedance, i.e. 40 $cm^3$ reservoir, no pressure node exists in the APA. However, for relatively small compliance impedance, i.e. 260 $cm^3$ reservoir, a small acoustic resistance may lead to occurrence of the pressure node.

Additionally, in abovementioned figures, there are no experimental data in the acoustic resistance range of $6.5\times10^7$~$1.8\times10^8$ Pa·s/$m^3$ for 260 $cm^3$ reservoir, and neither experimental data with the acoustic resistance below $2.1\times10^8$ Pa·s/$m^3$ for 40 $cm^3$ reservoir. It is because the system operation transited from fundamental-frequency mode to the second harmonic mode in the two cases. The second harmonic mode resulted in roughly doubled operating frequency, reduced pressure ratio and acoustic power delivered to the RC load, which are not expected for a good system performance. The possible reason for the frequency transition may be that the acoustic power dissipated in the whole thermoacoustic system is larger than the maximal acoustic power that could be generated in the stack at fundamental frequency. The mechanism and restraining methods of the frequency transition need to be further studied.

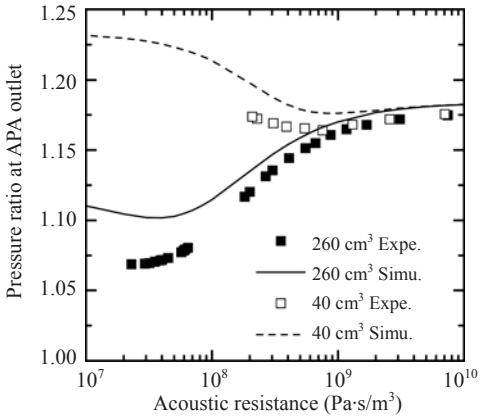


**Fig.12 Pressure ratio at APA's outlet**

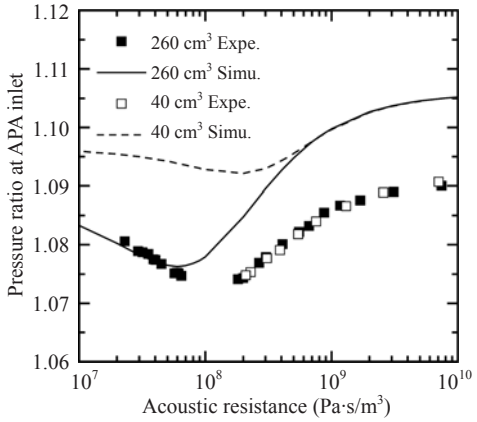


**Fig.13 Pressure ratio at APA's inlet**

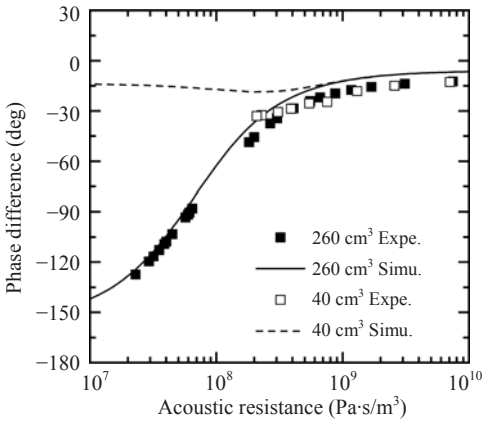


**Fig.14 Phase difference ($Phase_{inlet}-Phase_{outlet}$) of pressure waves at APA's outlet and inlet**

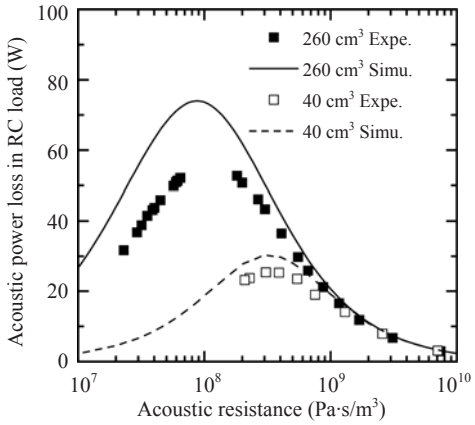


**Fig.15 Acoustic power loss in RC load**

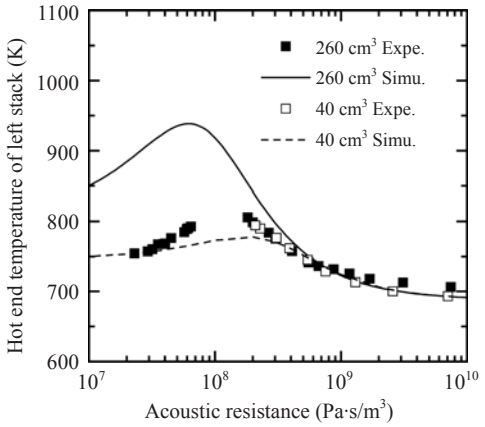


**Fig.16 Hot end temperature of left stack**

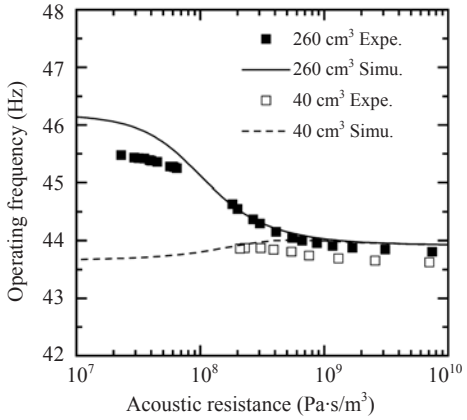


**Fig.17 Operating frequency**

## CONCLUSION

A standing-wave thermoacoustic engine driving an RC load through an APA is simulated to study the influence of RC load impedance on system's operation. Simulation results indicate that the distribution of pressure amplitude and velocity amplitude in APA resembles a standing-wave acoustic field, and is significantly affected by the impedance of RC load. In the case of relatively small acoustic resistances, e.g.

below $1\times10^6$ Pa·s/m$^3$ as in the simulation, compliance impedance of RC load dominates the system's operation, and there is a critical compliance impedance leading to the occurrence of pressure node and velocity antinode in APA. A compliance impedance close to the critical value leads to higher pressure ratio at APA's outlet, more acoustic power loss in APA and higher hot end temperature of stack, but lower pressure ratio at APA's inlet, less acoustic power generation and acoustic power loss in engine. For relatively large acoustic resistance, e.g. above $1\times10^9$ Pa·s/m$^3$ as in the simulation, compliance impedance has little influence on system's performance, and a rise of acoustic resistance results in an increase of above-mentioned operating parameters except hot end temperature of stack. A "peak" of acoustic power output occurs under the acoustic resistance between $1\times10^6$ Pa·s/m$^3$ and $1\times10^9$ Pa·s/m$^3$, comparable with the compliance impedance. A higher "peak" is achieved with the compliance impedance below the critical value. In addition, the acoustic resistance for the maximum acoustic power output is unequal to the compliance impedance of RC load in thermoacoustic system employing an APA, which is different from the situation without APA.

Experiment of the standing-wave thermoacoustic engine driving an RC load through an APA has been carried out to verify the simulation. The comparison between computed results and experimental data indicates that the simulation can roughly predict the system operation in the fundamental-frequency mode.

## References


Arman, B., Wollan, J.J., Swift, G.W., Backhaus, S., 2003. Thermoacoustic Natural Gas Liquefiers and Recent Developments. Cryogenics and Refrigeration, Proceedings of ICCR'2003, p.123-127.

Bao, R., Chen, G.B., Tang, K., Cao, W.H., Jin, T., 2006a. Thermoacoustically driven pulse tube refrigeration below 80 K by introducing an acoustic pressure amplifier. *Applied Physics Letters*, **89**(21):211915. [doi:10.1063/1.2387939]

Bao, R., Chen, G.B., Tang, K., Jia, Z.Z., Cao, W.H., 2006b. Effect of RC load on performance of thermoacoustic engine. *Cryogenics*, **46**(9):666-671. [doi:10.1016/j.cryogenics.2006.04.002]

Dai, W., Luo, E.C., Hu, J.Y., Chen, Y.Y., 2005. A novel coupling configuration for thermoacoustically-driven pulse tube coolers: Acoustic amplifier. *Chinese Science Bulletin*, **50**(18):2112-2114. [doi:10.1360/982005-482]

Duthil, P., Baltean Carlès, D., Bétrancourt, A., François, M.X., Yu, Z.B., Thermeau, J.P., 2006. Experiments and valve modeling in thermoacoustic device. *Advances in Cryogenic Engineering*, **51**(B):1095-1102.

Hu, J.Y., Luo, E.C., Dai, W., Zhou, Y., 2007. A heat-driven thermoacoustic cryocooler capable of reaching below liquid hydrogen temperature. *Chinese Science Bulletin*, **52**(4):574-576. [doi:10.1007/s11434-007-0104-5]

Matsubara, Y., Dai, W., Onishi, T., Kushino, A., Sugita, H., 2003. Thermally Actuated Pressure Wave Generators for Pulse Tube Cooler. Cryogenics and Refrigeration, Proceedings of ICCR'2003, p.57-60.

Nguyen, C.T., Yeckley, A.J., Schieb, D.J., Haberbusch, M.S., 2004. Hydrogen/oxygen propellant densifier thermoacoustic Stirling heat engine. *Advances in Cryogenic Engineering*, **49**(B):1703-1709.

Swift, G.W., 2002. Thermoacoustics: A Unifying Perspective for Some Engines and Refrigerators. Acoustical Society of America Publications, Sewickley, PA.

Tang, K., Chen, G.B., Kong, B., 2004. A 115 K thermoacoustically driven pulse tube refrigerator with low onset temperature. *Cryogenics*, **44**(5):287-291. [doi:10.1016/j.cryogenics.2003.12.004]

Tang, K., Chen, G.B., Jin, T., Bao, R., Kong, B., Qiu, L.M., 2005. Influence of resonance tube length on performance of thermoacoustically driven pulse tube refrigerator. *Cryogenics*, **45**(3):185-191. [doi:10.1016/j.cryogenics.2004.10.002]

Tang, K., Chen, G.B., Jin, T., Bao, R., Li, X.M., 2006. Performance comparison of thermoacoustic engines with constant-diameter resonant tube and tapered resonant tube. *Cryogenics*, **46**(10):699-704. [doi:10.1016/j.cryogenics.2006.04.006]

Tang, K., Bao, R., Chen, G.B., Qiu, Y., Shou, L., Huang, Z.J., Jin, T., 2007. Thermoacoustically driven pulse tube cooler below 60 K. *Cryogenics*, **47**(9-10):526-529. [doi:10.1016/j.cryogenics.2007.04.003]

Yu, G.Y., Luo, E.C., Dai, W., Wu, Z.H., 2007. An energy-focused thermoacoustic-Stirling heat engine reaching a high pressure ratio of 1.40. *Cryogenics*, **47**(2):132-134. [doi:10.1016/j.cryogenics.2006.12.001]